

Infall of gas as the formation mechanism of stars up to 20 times more massive than the Sun

Maria T. Beltrán¹, Riccardo Cesaroni², Claudio Codella³,
Leonardo Testi², Ray S. Furuya⁴ & Luca Olmi³

October 12, 2018

¹ Departament d'Astronomia i Meteorologia, Universitat de Barcelona, Av. Diagonal, 647, 08028, Barcelona, Catalunya, Spain

² Osservatorio Astrofisico di Arcetri, Largo E. Fermi 5, 50125 Firenze, Italy

³ Istituto di Radioastronomia, INAF, Sezione di Firenze, Largo E. Fermi 5, 50125 Firenze, Italy

⁴ Subaru Telescope, National Astronomical Observatory of Japan, 650 North Aohoku Place, Hilo, HI 96720, USA

Theory predicts and observations confirm that low-mass stars (like the Sun) in their early life grow by accreting gas from the surrounding material. But for stars ~ 10 times more massive than the Sun ($\sim 10 M_{\odot}$), the powerful stellar radiation is expected to inhibit accretion¹ and thus limit the growth of their mass. Clearly, stars with masses $> 10 M_{\odot}$ exist, so there must be a way for them to form. The problem may be solved by non-spherical accretion^{2,3}, which allows some of the stellar photons to escape along the symmetry axis where the density is lower. The recent detection of rotating disks⁴⁻⁶ and toroids⁷ around very young massive stars has lent support to the idea that high-mass ($\gtrsim 8 M_{\odot}$) stars could form in this way. Here we report observations of an ammonia line towards a high-mass star forming region. We conclude from the data that the gas is falling inwards towards a very young star of $\sim 20 M_{\odot}$, in line with theoretical predictions of non-spherical accretion.

In the work we report here, we have revealed the simultaneous presence of three elements in the same massive object: outflow, rotation, and infall. Although evidence of circumstellar disks or toroids in massive objects had been provided by a number of observational studies^{4–10} (see Ref. 11 for a review), it remained to be proved that these are accretion structures, sustaining the growth of the central star(s). Evidence of infall had been found only in a very limited number of massive objects^{12–17}, but in no case had the simultaneous presence of rotation, outflow, and infall towards an O-B (proto)star been established. Our findings hence represent a substantial advance in this field.

The source under investigation is G24.78+0.08, a massive star forming region located at a distance of 7.7 kpc, studied by us in great detail^{7,18–21}. This contains a cluster of Young Stellar Objects (YSOs), three of them associated with rotating toroids. In one of these, G24 A1, the presence of an early-type star is witnessed by a hypercompact HII region (M.T.B. *et al.*, manuscript in preparation) with a diameter $\lesssim 0''.2$ ($\lesssim 1,500$ AU) and located at the geometrical centre of the toroid (see Fig. 1). The continuum spectrum resembles that of a classical (Strömgen) HII region around a zero-age main sequence star of spectral type O9.5¹⁸, corresponding to a mass of $\sim 20 M_{\odot}$, a luminosity of $\sim 33,000 L_{\odot}$ and a Lyman continuum of 5×10^{47} sec⁻¹. Being the HII region very bright at centimeter wavelengths ($\gtrsim 2,000$ K), it is easy to observe the colder molecular gas (~ 100 K) in absorption against it. If the toroid is not only rotating, but also accreting onto the central star, one expects to see absorption at positive velocities (i.e. red-shifted by Doppler effect) relative to the stellar velocity^{12–15}. The latter (~ 110.8 km s⁻¹) is equal to the mean velocity of the gas in the toroid, estimated from molecules whose lines are not affected by absorption²¹, such as methyl cyanide (CH₃CN).

With this in mind, we observed simultaneously the continuum emission and the ammonia (NH₃) (2,2) inversion transition at 1.3-cm wavelength using the Very Large Array (VLA) interferometer of the National Radio Astronomy Observatory (NRAO) in the B configuration. As expected, the line is seen in absorption towards the continuum of the HII region: this is shown by the white contours in Fig. 1a, where one can also see the emission (black contours) detected towards the adjacent toroid G24 A2, not discussed here. Clearly, the peak of absorption as well as the peak of the 1.3-cm continuum emission (i.e. of the HII region) lie at the center of the toroid previously imaged by us (yellow line) and along the axis of the associated bipolar outflow (black arrows). The velocity gradient in the rotating toroid is shown in Fig. 1b, overlaid on an image and contour map of the CH₃CN emission at 1.4-mm wavelength previously obtained by us^{7,21} with the IRAM Plateau de Bure interferometer (PdBI) in

the most extended configuration.

Figure 2 illustrates the most important finding of our study. In order to understand this figure, one must keep in mind that the NH_3 inversion transitions have a complex structure, made of a “main” component and four “hyperfine satellites”. The former line is intrinsically stronger than the latter ones by a factor ~ 14 , so that, roughly speaking, emission in the main line is representative of lower gas densities, whereas the satellites trace the densest material. In Fig. 2 we show position-velocity plots for both the main line (Fig. 2a) and the mean satellite emission (Fig. 2b), where the offset in position is measured along the plane of the rotating toroid. In Fig. 2c we show the same plot for the $\text{CH}_3\text{CN}(12-11)$ $K = 3$ line which was used by us to trace rotation in the toroid⁷. Three considerations are in order: 1) Towards the hypercompact HII region, the satellite absorption is strongly biased towards positive velocities, i.e. red-shifted with respect to the velocity of the star; 2) The NH_3 main line is seen in absorption at both positive and negative velocities, but the blue-shifted absorption is fainter, broader, and more optically thin than the red-shifted one; 3) The velocity gradient seen in the CH_3CN line (outlined by the green line in Fig. 2c), is detected also in the NH_3 main line (green line across the two emission peaks in Fig. 2a), thus confirming the presence of rotation.

The important conclusion is that the densest gas seen in the satellite absorption is moving away from the observer at a speed of $\sim 2 \text{ km s}^{-1}$ (see Fig. 2b) towards the hypercompact HII region, namely towards the star. This fact proves the presence of infall onto the O-type star at the center of the toroid. On the other hand, the faint and broad blue-shifted absorption seen in the main line is very likely due to the low-column density gas in the lobe of the molecular outflow that is moving towards the observer: this is indicated by the lower main line/satellite ratio (i.e. lower optical depth) observed in the blue line wing with respect to the one in the red-shifted absorption. Incidentally, we note that the broad blue-shifted absorption can be used to discriminate between sources G24 A1 and G24 A2 as origin of the outflow. Since the blue-shifted lobe is directed towards NW¹⁹, it cannot originate from G24 A2 or it would not pass in front of G24 A1. We hence believe that the star in G24 A1 is powering the flow.

What are the implications of the detection of infall in G24 A1? Using the properties of the $\text{NH}_3(2,2)$ transition and an estimate of the gas temperature²¹, one can derive the column density of the infalling gas, N_{H_2} , from the ratio between the main line intensity and that of the satellites²², assuming an NH_3 abundance relative to H_2 of 10^{-6} – 10^{-7} (refs 18, 23). From N_{H_2} and the infall

velocity, $v_{\text{inf}} \simeq 2 \text{ km s}^{-1}$, assuming free-fall one obtains the mass accretion rate onto the star inside a solid angle Ω : $\dot{M}_{\text{acc}} \simeq \Omega/(4\pi) (4 \times 10^{-4} - 10^{-2}) M_{\odot} \text{ yr}^{-1}$. A detailed derivation of the mass accretion rate is presented in Supplementary Information. The range of values reflects the uncertainty on N_{H_2} and on the radius at which v_{inf} is measured. Noticeably, \dot{M}_{acc} is much larger than the critical rate above which formation of an HII region is inhibited²⁴ if accretion is spherically symmetric (i.e. for $\Omega = 4\pi$). For an O9.5 star this is $\dot{M}_{\text{inh}} \simeq 8 \times 10^{-6} M_{\odot} \text{ yr}^{-1}$, much less than \dot{M}_{acc} : this should suffice to prevent the formation of an HII region. The fact that, instead, an HII region is detected can be explained only if the accretion is not spherically symmetric ($\Omega < 4\pi$), which in turn supports the existence of a circumstellar disk-like structure, detected by us on a larger scale as a toroid.

It is also interesting to estimate the rate needed for the ram pressure to overcome the thermal pressure of the HII region ($\dot{M}_{\text{HII}} \simeq \Omega/(4\pi) 2 \times 10^{-4} M_{\odot} \text{ yr}^{-1}$). This has been obtained assuming an electron density and diameter of the HII region respectively of $\sim 10^6 \text{ cm}^{-3}$ ⁽¹⁸⁾ and $0''.2$ (see above) or 0.0075 pc . One sees that $\dot{M}_{\text{acc}} \geq \dot{M}_{\text{HII}}$ independently of Ω , which indicates that the accretion is large enough to brake or slow down the expansion of the HII region through the toroid. This conclusion is strengthened if one takes into account the effect of stellar gravity, likely non-negligible in such a small HII region. Detailed models support this conclusion, and predict that hypercompact HII regions could be long lived because of trapping of the ionized gas²⁵ owing to infall in the gravitational field of the star.

We now consider the effect of our findings on current theories of massive star formation. Stars as massive as $\sim 8 M_{\odot}$ are believed to reach the zero-age main sequence still accreting. At this stage, their powerful radiation pressure appears to be strong enough to halt the infalling material^{1,26}, which should inhibit further growth of the star beyond the limit of $\sim 8 M_{\odot}$. In order to solve this problem merging of low-mass stars has been proposed²⁷, although – even in the most favourable case of induced binary mergers – to be effective this scenario requires very large stellar densities, at least of the order of $10^6 \text{ stars pc}^{-3}$. Increasing the mass accretion rate may be a viable theoretical solution to overcome the radiation pressure with the ram pressure of the infalling material. Moreover, this would solve the lifetime problem²⁸ related to the fact that with accretion rates typical of low-mass stars ($10^{-5} M_{\odot} \text{ yr}^{-1}$) the time needed to form a star $> 10 M_{\odot}$ would be too long ($> 10^6 \text{ yr}$), comparable to the entire lifetime of the star. Higher rates can be achieved either by assuming a large turbulent pressure^{28,29} in the molecular cores forming O-B type stars, or deepening the gravitational well³⁰ around a massive star

by surrounding it with a tight cluster of lower mass companions. Non-spherical accretion may also soften the problem^{2,3}: focusing accretion into a circumstellar disk reduces significantly the radiation pressure force along the equator by beaming the radiation in the direction of the poles.

In our case, direct accretion onto the central massive (proto-)star has not yet been detected, so that the system may be in a (relatively) late phase, when the final mass of the central object has been assembled and the infalling material is being deflected in the outflow instead of being accreted. Nevertheless, our detection of infall towards G24 A1 is an important milestone towards an observational constraint of the theoretical models. In fact, even if the very accretion phase were finished, the presence of a rotating toroid infalling on a hypercompact HII region, located at the base of a powerful collimated bipolar flow, is broadly in agreement with the expectations of the non-spherical accretion scenario for the formation of massive stars. Our results thus suggest that this is a plausible mechanism for the formation of stars at least as massive as $20 M_{\odot}$. More ‘exotic’ mechanisms (such as stellar mergers) might still be required to form stars of even higher mass.

1. Kahn, F. D. Cocoons around early-type stars. *Astron. Astrophys.* **37**, 149-162 (1974).
2. Yorke, H. W. & Sonnhalter, C. On the formation of massive stars. *Astrophys. J.* **569**, 846-862 (2002).
3. Krumholz, M. R., McKee, C. F., & Klein, R. I. How protostellar outflows help massive stars form. *Astrophys. J.* **618**, L33-L36 (2005).
4. Cesaroni, R. *et al.* A study of the Keplerian accretion disk and precessing outflow in the massive protostar IRAS 20126+4104. *Astron. Astrophys.* **434**, 1039-1054 (2005).
5. Chini, R. *et al.* The formation of a massive protostar through the disk accretion of gas. *Nature* **429**, 155-157 (2004).
6. Patel, N. *et al.* A disk of dust and molecular gas around a high-mass protostar. *Nature* **437**, 109-111 (2005).
7. Beltrán, M. T. *et al.* Rotating disks in high-mass young stellar objects. *Astrophys. J.* **601**, L187-L190 (2004).
8. Cesaroni, R., Felli, M., Testi, L., Walmsley, C. M. & Olmi, L. The disk-outflow system around the high-mass (proto)star IRAS 20126+4104. *Astron. Astrophys.* **325**, 725-744 (1997).

9. Jiang, Z. *et al.* A circumstellar disk associated with a massive protostellar object. *Nature* **437**, 112-115 (2005).
10. Cesaroni, R. in *Massive Star Birth: A Crossroads of Astrophysics* (eds Cesaroni, R., Felli, M., Churchwell, E. & Walmsley, M.), 59-69 (Proc. *IAU Symp.* **227**, Univ. Press, Cambridge 2005).
11. Cesaroni, R. Outflow, infall, and rotation in high-mass star forming regions. *Ap&SS* **295**, 5-17 (2005).
12. Ho, P. T. P. & Haschick, A. D. Molecular clouds associated with compact HII regions. III. Spin-up and collapse in the core of G10.6–0.4. *Astrophys. J.* **304**, 501-514 (1986).
13. Keto, E. R., Ho, P. T. P. & Haschick, A. D. Temperature and density structure of the collapsing core of G10.6–0.4. *Astrophys. J.* **318**, 712-728 (1987).
14. Zhang, Q. & Ho, P. T. P. Dynamical collapse in W51 massive cores: NH₃ observations. *Astrophys. J.* **488**, 241-257 (1997).
15. Hofner, P., Peterson, S. & Cesaroni, R. Ammonia absorption toward the ultracompact HII regions G45.12+0.13 and G45.47+0.05. *Astrophys. J.* **514**, 899-908 (1999).
16. Sollins, P. & Ho, P. T. P. The molecular accretion flow in G10.6–0.4. *Astrophys. J.* **630**, 987-995 (2005).
17. Zhang, Q. in *Massive Star Birth: A Crossroads of Astrophysics* (eds Cesaroni, R., Felli, M., Churchwell, E. & Walmsley, M.), 135-144 (Proc. *IAU Symp.* **227**, Univ. Press, Cambridge 2005).
18. Codella, C., Testi, L. & Cesaroni, R. The molecular environment of H₂O masers: VLA ammonia observations. *Astron. Astrophys.* **325**, 282-294 (1997).
19. Furuya, R. S. *et al.* G24.78+0.08: A cluster of high-mass (proto)stars. *Astron. Astrophys.* **390**, L1-L4 (2002).
20. Cesaroni, R., Codella, C., Furuya, R. S. & Testi, L. Anatomy of a high-mass star forming cloud: The G24.78+0.08 (proto)stellar cluster. *Astron. Astrophys.* **401**, 227-242 (2003).
21. Beltrán, M. T. *et al.* A detailed study of the rotating toroids in G31.41+0.31 and G24.78+0.08. *Astron. Astrophys.* **435**, 901-925 (2005).
22. Ungerechts, H., Winnewisser, G. & Walmsley, C. M. Ammonia observations and temperatures in the S140/L1204 molecular cloud. *Astron. Astrophys.* **157**, 207-216 (1986).
23. Cesaroni, R., Churchwell, E., Hofner, P., Walmsley, C. M. & Kurtz, S. Hot ammonia towards compact HII regions. *Astron. Astrophys.* **288**, 903-920 (1994).

24. Walmsley, M. Dense cores in molecular clouds (*Rev. Mexicana Astron. Astrofis., Conf. Ser.*, Vol. **1**, 137–148 (1995).
25. Keto, E. On the evolution of ultracompact HII regions. *Astrophys. J.* **580**, 980-986 (2002).
26. Wolfire, M. G. & Cassinelli, J. P. Conditions for the formation of massive stars. *Astrophys. J.* **319**, 850-867 (1987).
27. Bonnell, I. A. & Bate, M. R. Binary systems and stellar mergers in massive star formation. *Mon. Not. R. Astron. Soc.* **362**, 915-920 (2005).
28. McKee, C. F. & Tan, J. C. The Formation of Massive Stars from Turbulent Cores. *Astrophys. J.* **585**, 850-871 (2003).
29. McKee, C. F. & Tan, J. C. Massive star formation in 100,000 years from turbulent and pressurized molecular clouds. *Nature* **416**, 59-61 (2002).
30. Bonnell, I. A., Vine, S. G. & Bate, M. R. Massive star formation: nurture, not nature. *Mon. Not. R. Astron. Soc.* **349**, 735-741 (2004).

Supplementary Information is linked to the online version of the paper at www.nature.com/nature.

Acknowledgments NRAO is operated by Associated University, Inc., under contract with the National Science Foundation. It is a pleasure to thank Dr. Paul Ho and another anonymous referee for their constructive criticisms which greatly improved the presentation of our results.

Correspondence and requests for materials should be addressed to M.T.B. (mbeltran@am.ub.es).

Figure 1: **Absorption and emission by molecular gas towards the hypercompact HII region G24 A1.** **a**, Map of the intensity integrated under the $\text{NH}_3(2,2)$ inversion line (colour image). Black contours indicate positive intensity (emission), while white contours are negative (absorption). The white filled circle marks the position of the hypercompact HII region detected in the continuum emission at 1.3-cm wavelength¹⁷ (Beltrán et al. in preparation). The black arrows outline the direction of the bipolar outflow, ejected along the axis of the disk. The disk plane is denoted by the yellow line. Note the deep absorption towards the HII region, at the center of the toroid. The final maps have been reconstructed with a circular synthesized beam of $0''.8 \times 0''.8$, which is represented by the hatched circle. The $1\text{-}\sigma$ noise of the integrated $\text{NH}_3(2,2)$ line is $0.6 \text{ mJy beam}^{-1}$. Contour levels start at a $\pm 3\text{-}\sigma$ level and vary by $3\text{-}\sigma$ (positive contours) and $12\text{-}\sigma$ (negative contours). **b**, Map (image and contours) of the intensity integrated under the $\text{CH}_3\text{CN}(12\text{--}11) K = 3$ line²¹ outlining the toroids in G24 A1 and G24 A2 (the latter is not discussed in this article). The colour scale corresponds to the velocity field of the toroid in G24 A1: note how the velocity changes gradually from red-shifted to blue-shifted, consistently with rotation about the outflow axis. A velocity gradient, similar to that in G24 A1, has also been detected⁷ in the other core G24 A2, but is neither shown nor discussed here. Symbols have the same meaning as above. The resulting synthesized beam is $1''.2 \times 0''.5$ at $\text{PA} = -174^\circ$ and is represented by the hatched ellipse at the bottom right. The $1\text{-}\sigma$ noise of the intensity integrated under the $\text{CH}_3\text{CN}(12\text{--}11) K = 3$ line is 35 mJy beam^{-1} . Contour levels start at $0.25 \text{ Jy beam}^{-1}$ and increase by 0.2 Jy beam^{-1} . δ , declination; α , right ascension.

Figure 2: **Velocity field in the massive toroid G24 A1.** **a**, Position-velocity plot of the $\text{NH}_3(2,2)$ main line intensity. The positional cut is made along the plane of the disk, $\text{PA} = -135^\circ$, namely along the yellow line in Fig. 1. Both offset and velocity are computed with respect to the star. Black and white contours correspond respectively to emission and absorption. The continuum has been subtracted from the line emission. The $1\text{-}\sigma$ noise is 1 mJy beam^{-1} . Contour levels start at a $3\text{-}\sigma$ level and increase by $3\text{-}\sigma$ (positive contours) and $6\text{-}\sigma$ (negative contours). The error bars denote the angular and spectral resolution. The original spectral resolution was $\sim 0.31 \text{ km s}^{-1}$, which was degraded by a factor 2 to improve the S/N by averaging pairs of adjacent channels. Note the velocity gradient outlined by the green line. **b**, As **a** but for the $\text{NH}_3(2,2)$ satellite line. Note how the

absorption peak is red-shifted with respect to the stellar velocity. **c**, As **a** but for the $\text{CH}_3\text{CN}(12-11)$ $K = 3$ line: the velocity gradient outlined by the green line is indicative of rotation²¹. The $1-\sigma$ noise is 48 mJy beam^{-1} .

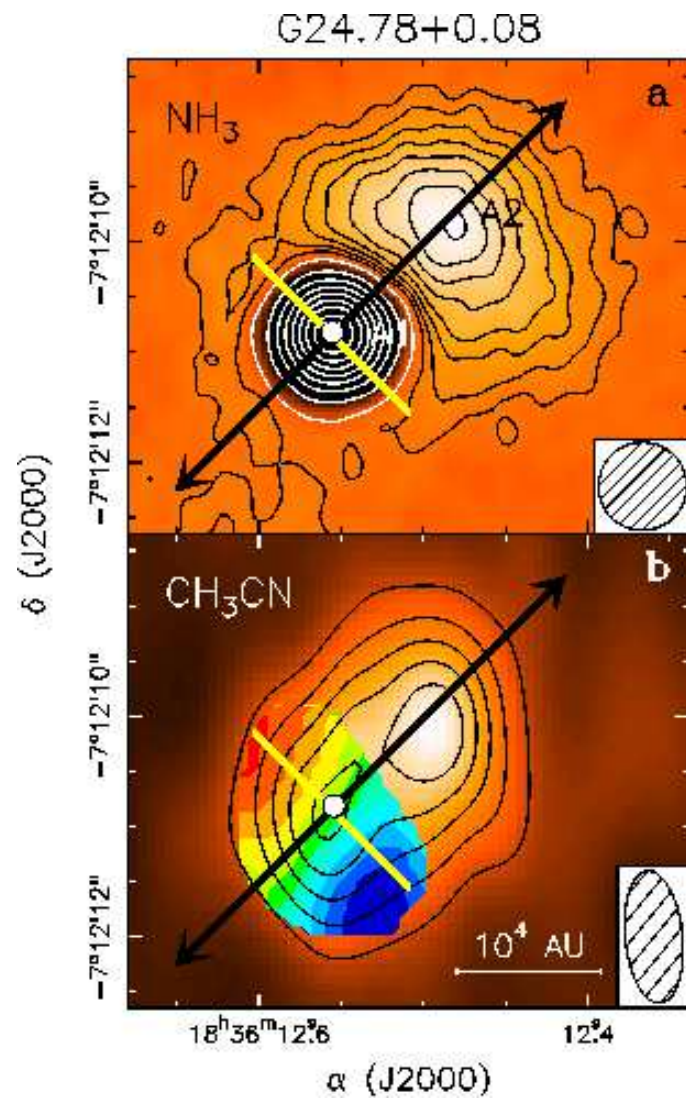


Figure 1:

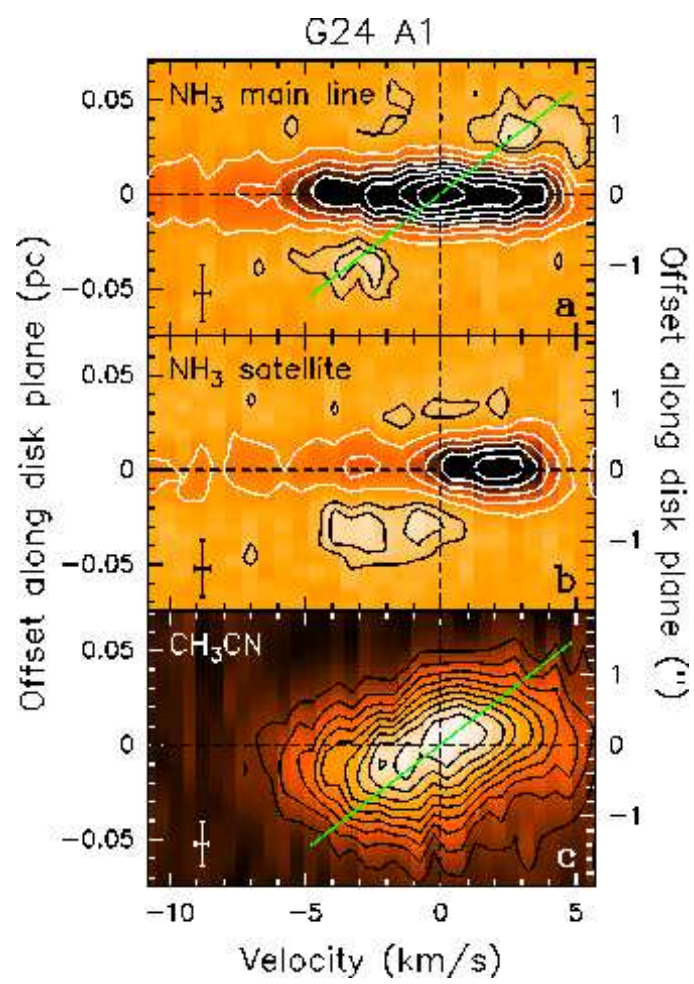


Figure 2: